Journal of Neurology
https://doi.org/10.1007/s00415-021-10762-9

ORIGINAL COMMUNICATION

Semi-automated assessment of the principal diffusion direction in the corpus callosum: differentiation of idiopathic normal pressure hydrocephalus from neurodegenerative diseases

Maria Eugenia Caligiuri[1] · Andrea Quattrone[2] · Alessandro Mechelli[2] · Domenico La Torre[3] · Aldo Quattrone[1]

Received: 17 May 2021 / Revised: 22 July 2021 / Accepted: 17 August 2021

Abstract

Background Idiopathic normal pressure hydrocephalus (iNPH) shares clinical and radiological features with progressive supranuclear palsy (PSP) and Alzheimer's disease (AD). Corpus callosum (CC) involvement in these disorders is well established on structural MRI and diffusion tensor imaging (DTI), but alterations overlap and lack specificity to underlying tissue changes.

Objective We propose a semi-automated approach to assess CC integrity in iNPH based on the spatial distribution of DTI-derived principal diffusion direction orientation (V1).

Methods We processed DTI data from 121 subjects (Site1: iNPH = 23, PSP = 27, controls = 14; ADNI: AD = 35, controls = 22) to obtain V1, fractional anisotropy (FA) and mean diffusivity (MD) maps. To increase the estimation accuracy of DTI metrics, analyses were restricted to the midsagittal CC portion (±6 slices from midsagittal plane). Group-wise comparison of normalized altered voxel count in midsagittal CC was performed using Kruskal–Wallis tests, followed by post hoc comparisons (Bonferroni-corrected $p < 0.05$). ROC analysis was used to evaluate the diagnostic power of DTI alterations compared to callosal volume.

Results We found specific changes of V1 distribution in CC splenium of iNPH compared to AD and PSP, while MD and FA showed patterns of alterations common to all disorders. ROC curves showed that, compared to splenial volume, V1 represented the most accurate marker of iNPH diagnosis versus AD and PSP.

Conclusions Our results provide evidence that V1 is a powerful biomarker for distinguishing patients with iNPH from patients with AD or PSP. Indeed, our findings also provide more specific insight into the pathophysiological mechanisms that underlie tissue damage across iNPH and its mimics.

Keywords Diffusion tensor imaging · Principal diffusion direction · Corpus callosum · Idiopathic normal pressure hydrocephalus · Alzheimer's disease · Progressive supranuclear palsy

Introduction

Idiopathic normal pressure hydrocephalus (iNPH) is a neurological disorder affecting the elderly population with symptoms that can impair motor, autonomic and cognitive domains. Its clinical presentation alone, however, is not sufficient to reach an early diagnosis and subsequently recommend shunt surgery. In fact, the most common symptoms of iNPH (represented by the clinical triad: gait disturbance, cognitive impairment and urinary incontinence) are not specific and can be also found in patients affected by other neurodegenerative diseases, such as Alzheimer's disease (AD) and progressive supranuclear palsy (PSP).

Maria Eugenia Caligiuri and Andrea Quattrone have contributed equally.

✉ Aldo Quattrone
quattrone@unicz.it

[1] Neuroscience Research Center, University "Magna Graecia", Viale Europa, 88100 Catanzaro, Italy

[2] Institute of Neurology, University "Magna Graecia", Catanzaro, Italy

[3] Institute of Neurosurgery, University "Magna Graecia", Catanzaro, Italy

Published online: 24 August 2021

These disorders also share radiological signs, in addition to clinical ones: magnetic resonance imaging (MRI) features suggestive of PSP, such as the qualitative hummingbird sign and the quantitative, automated magnetic resonance parkinsonism index [1, 2], can also be found in iNPH patients, while vertical supranuclear gaze palsy, the most specific sign of PSP, does not necessarily manifest early in the course of the disease, especially in milder phenotypes. A recent study has shown that volumetric and linear measures of ventricular dilation (automated ventricular volumetry and magnetic resonance hydrocephalic index) can differentiate iNPH from PSP with up to 98.4% accuracy [3]. However, severe ventricular dilation is frequently observed in patients with AD and this, coupled with the presence of cognitive impairment in both diseases, can be a confounding factor that further hampers the early and correct identification of patients with iNPH.

The corpus callosum (CC) is a key region of the brain, connecting homo- and heterotopic regions of the cerebral hemispheres, and also represents the upper boundary of the lateral ventricles. Structural MRI and diffusion tensor imaging (DTI) studies have highlighted the involvement of this bundle in iNPH, AD and PSP [4–7]. Despite that all these disorders have different, sometimes unknown, etiologies (i.e., age-related causes, amyloid burden, tauopathies), existing studies reported similar patterns of atrophy and DTI alterations across the callosal region, which are likely driven by different pathological mechanisms (e.g., overproduction of cerebrospinal fluid, neurodegeneration, abnormal deposition of amyloid-beta or tau protein).

These commonalities in alteration patterns are not very surprising, since the diagnostic potential of commonly used DTI scalars, namely fractional anisotropy and mean diffusivity (FA, MD), is strongly limited by their lack of specificity to underlying pathological processes [8]. Thus, it is important to thoroughly investigate also other properties of the diffusion tensor, such as the orientation of the tensor's principal eigenvector (V1, i.e., the principal diffusion direction), which could provide additional insight into the nature of tissue changes. Theoretical frameworks to quantitatively assess V1 have been described, but they have not been widely applied to clinical settings yet [9, 10].

Among all regions of the brain, CC represents a valuable window of observation for V1 characterization: first, the varied nature of callosal fibers [11] might bring information not only on the bundle itself, but also indirectly on the status of cortical regions connected by specific fibers; second, given its size and location, the CC is also particularly easy to identify and coarsely align across different subjects, even in the presence of severe atrophy or other disease-related deformations; last, but *not* least, the strong directionality of the bundle should warrant that the estimation of voxel-wise fiber orientation is sufficiently reliable, even dealing with diffusion-weighted sequences suitable for clinical practice—i.e., single shell with a relatively low number of diffusion directions. In fact, the bundle runs in the mediolateral direction, especially in its midsagittal portion: by focusing on this section, the uncertainty in DTI measurements of voxels with different populations of crossing fibers can be limited.

In this study, we propose a semi-automated approach to assess CC integrity at the individual level, based on the spatial distribution of V1 in the midsagittal portion of CC. We subsequently addressed the clinical challenge of differentiating iNPH from AD and PSP, by characterizing V1 alterations across different diseases and compare their usefulness as diagnostic tool, compared to other more common disease-related MRI metrics, such as callosal volume.

Materials and methods

Patients

Twenty-three patients with possible iNPH with MRI support, 27 patients with probable PSP (14 with PSP–Richardson's syndrome and 13 with PSP-P), 35 patients with probable AD and 37 healthy control subjects (14 from our site and 23 from the ADNI database) were enrolled in the current study. iNPH and PSP patients were recruited consecutively between 2017 and 2019 among those referred to the Institute of Neurology at the University of Catanzaro, Italy. Healthy control subjects were enrolled as volunteers at the same institution. Diagnosis of possible iNPH with MRI support was established according to international diagnostic guidelines [12]. Thirteen of 23 iNPH patients subsequently underwent shunt surgery with clinical benefit and were reclassified as definite iNPH. All MRI data of the 23 INPH patients analyzed in our study were obtained before the shunt procedure, when patients were still classified as possible iNPH with MR support. Clinical diagnosis of probable PSP was established according to recent international diagnostic criteria by a physician with > 10 years of experience in movement disorders [13]. All patients underwent a detailed clinical assessment, including the UPDRS-Motor Examination, the Mini-Mental State Examination (MMSE) and the iNPH grading scale. Exclusion criteria for our patients included: history of neuroleptic use within the previous 6 months, clinical features suggestive of other diseases, and MRI abnormalities such as lacunar infarctions in the basal ganglia and/or subcortical vascular lesions with diffuse periventricular signal alterations. In addition, none of the PSP patients showed Evans index > 0.32 associated with callosal angle < 100°, a combination of MRI biomarkers strongly suggestive of iNPH. None of the iNPH patients had a history of subarachnoid hemorrhage, meningitis, head injury or congenital hydrocephalus, vertical ocular dysfunction, or radiological

evidence of stenosis of the cerebral aqueduct. None of the control subjects had a history of neurological, psychiatric, or other major medical illnesses.

Patients with AD were drawn from Alzheimer's Disease Neuroimaging Initiative (ADNI) cohort. ADNI data were obtained through the University of Southern California's Laboratory of Neuroimaging (LONI) data repository (http://adni.loni.ucla.edu/). Institutional Review Board approval and written informed consent were obtained at each of the participating institutions. The ADNI was launched in 2003 as a public–private partnership, led by Principal Investigator Michael W. Weiner, MD. The primary goal of ADNI has been to test whether serial magnetic resonance imaging (MRI), positron emission tomography (PET), other biological markers, and clinical and neuropsychological assessment can be combined to measure the progression of mild cognitive impairment (MCI) and early AD. Detailed inclusion/exclusion criteria for AD patients can be found on the ADNI website [14]. In this study, we selected patients with AD according to the following criteria: (i) 'axial DTI' acquisition, with the same acquisition parameters across centers, was available at baseline (in particular, number of axial slices); (ii) quality of the MRI acquisition, assessed by trained experts from the Mayo Clinic, was deemed acceptable [15]; (iii) cerebrospinal fluid biomarkers of AD were available (to strengthen reliability of diagnosis): in particular, patients showed evidence of reduced concentration of beta-amyloid$_{(1–42)}$ and increased concentration of tau and p-tau$_{181}$ in the CSF compared to controls [16]. As a result, 35 patients with AD and 23 healthy controls were selected from the ADNI database (all from ADNI2 project).

We considered demographic and clinical data, including sex, age at examination, age at disease onset, and MMSE score.

All local study procedures were carried out in accordance with the Declaration of Helsinki and ethical aspects were approved by the institutional review board (Magna Graecia University review board, Catanzaro, Italy). Each ADNI recruitment site received approval from an institutional review board or ethics committee on human experimentation before ADNI study initiation. Written informed consent for research was obtained from all individuals participating in the study.

MRI acquisition

A graphical representation of the proposed analysis, from the acquisition stage to statistical analysis, is shown in Fig. 1. All patients with iNPH and PSP, as well as 14 control subjects underwent brain MRI on a 3 T MR750 GE MRI scanner and an 8-channel head coil (Fig. 1a).

The acquisition protocol included the following sequences: whole-brain, 3D T1-weighted spoiled gradient recalled-echo imaging (BRAVO; TE/TR = 3.7/9.2 ms, flip angle = 12°, voxel size = 1 mm × 1 mm × 1 mm), diffusion tensor imaging (DTI; TE/TR = 81.4/10000 ms; $b = 0$ and 1000 s/mm^2, diffusion- weighting along 27 non-collinear gradient directions, matrix size = 128 × 128, 80 axial slices, number of b0 images = 4, NEX = 2, voxel size = 2 mm × 2 mm × 2 mm), and fast fluid-attenuated inversion recovery axial images (FLAIR; TR/TE = 9500/100 ms, matrix size = 512 × 512, FOV = 24 cm, 36 4-mm sections, gap = 0 mm).

All MRI series acquired at our center were examined to exclude scans with poor signal-to-noise ratio and/or brain abnormalities, following the procedures described on the ADNI website [17], to match the quality control of AD images (inclusion criterion was acceptable quality).

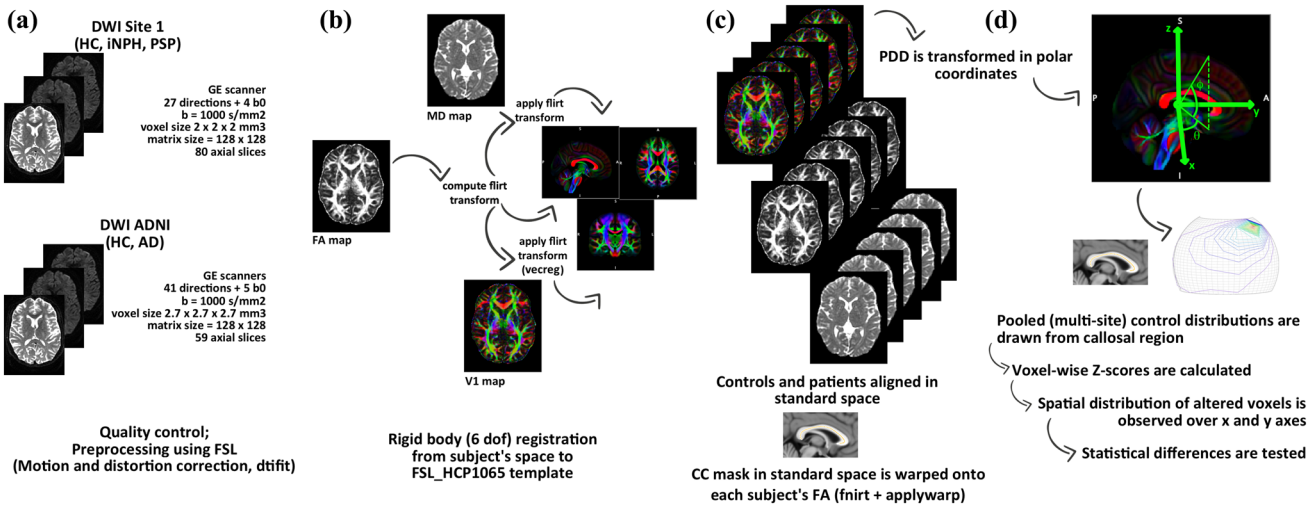

Fig. 1 DTI processing and analysis workflow

MRI series from the ADNI cohort were acquired on 3 T GE systems with an eight-channel head coil at ten different sites, using the following acquisition parameters: sagittal T1-weighted MRI, TR = 2300 ms, minimum full TE, TI = 900 ms, flip angle = 8°, FOV = 26 cm, with a 256 × 256 × 170 acquisition matrix in the *x*-, *y*-, and *z*-dimensions, yielding a voxel size of 1.0 mm × 1.0 mm × 1.2 mm; Axial DTI, b = 0 and 1000 s/mm^2, 41 diffusion-weighting directions, matrix size = 128 × 128, 59 axial slices, slice thickness = 2.7 mm, number of b0 images = 5, isotropic voxel size = 2.7 mm × 2.7 mm × 2.7 mm).

MRI post-processing

DTI processing was performed using FSL v. 6.0.3 [18]. Image distortions induced by eddy currents and head motion in the DTI data were corrected by applying a 3D full affine (mutual information cost function) alignment of each image to the mean no diffusion weighting (b0) image. After distortion corrections, DTI data were averaged and concatenated into either 28 volumes, for the locally acquired cohort, or 42 volumes, for the ADNI cohort. A diffusion tensor model was fit at each voxel, generating the standard DTI-derived scalar maps (mean, axial and radial diffusivity maps and fractional anisotropy maps) as well as vector images of the voxel-wise orientation of diffusion directions (V1, V2 and V3, the eigenvectors of the tensor).

As summarized in Fig. 1b, a 6-degrees-of-freedom rigid-body registration was applied to each individual FA map using FSL-FLIRT, with the FSL-HCP1065 1 mm FA template as a reference; the resulting linear transformation was subsequently applied on MD, axial (AxD) and radial diffusivity (rD) maps (using FSL-FLIRT) and on V1 and V2 maps (using FSL's *vecreg*). Due to orthogonality of V3 to both V1 and V2, V3 maps were not expected to add any information and thus were not analyzed [19]. At this point, all images were aligned in the same space, but no scaling or skewing was allowed on the maps, to prevent misregistration due to deformation of severely damaged brains (the majority of patients showed ventricle dilation).

To identify callosal voxels on each subject, a binary mask was obtained from the NatBrainLab Corpus Callosum atlas map [20]. A threshold of 0.3 was applied on the map to avoid less represented voxels [21]. To obtain individual masks of CC aligned in standard space, a nonlinear registration was computed between the standard template and each individual FA map. The resulting transform was applied to a standard CC mask using FSL's *applywarp* (Fig. 1c).

Using an in-house Matlab script, V1 and V2 maps were decomposed in polar coordinates (theta and phi angles) at each voxel (Fig. 1d). Subsequently, only voxels belonging to the callosal region were retained, selected by masking each individual's theta and phi maps with their CC mask. The reference distributions of theta and phi in CC were drawn by pooling the mean and standard deviation from the healthy control populations (14 from Site 1, 22 from ADNI data). Afterward, for each patient from the three disease groups, voxel-wise values of DTI scalars (FA, MD, AxD, rD) and eigenvectors (V1 and V2) were used to calculate z-scores. In particular, if a voxel's theta and phi values both exceeded mean ± 2.5 standard deviation of the control population, it was assigned value 1, thus creating for each variable a subject-specific binary mask of callosal values diverging from the reference distribution.

Finally, all T1 images were warped into standard space with the same approach used for FA maps, i.e., a 6-degrees-of-freedom rigid-body registration with MNI152 1 mm T1 template as a reference, to extract callosal volume using the same standard CC mask used in previous steps.

Statistical analysis

Differences in the distribution of sex were assessed using Chi-squared test. Other demographic and clinical variables were tested for normality using Shapiro–Wilk's test. Variables with normal distribution were compared across groups using ANOVA followed by pairwise *t* tests. Non-normally distributed variables, instead, were compared across groups using Kruskal–Wallis test, followed by pairwise Wilcoxon rank-sum test.

Subsequent MRI analyses were restricted to the midsagittal region of the CC (± 6 slices from the midsagittal plane); this was done to increase both anatomical correspondence across different subjects and head sizes, as well as accuracy of V1 estimation in a region where the direction of fibers is very well defined. Callosal volume limited to the considered midsagittal region was extracted from T1 images and normalized by the corresponding total intracranial volume, estimated using FSL-SIENAX. Concerning DTI analysis, as stated above, in the CC of each patient a voxel was considered altered if the z-scores of both angles, of FA or of diffusivity values exceeded 2.5 standard deviations above or below the controls' mean. The distribution of altered voxels was obtained for each subject: (i) along the mediolateral axis (x voxel coordinate, centered on the midsagittal plane ± 6 slices) of the three main CC subregions (splenium, body and genu); (ii) along the anteroposterior (y voxel coordinate) profile of the midsagittal CC. To compare the behavior of eigenvectors to that of the more common DTI-derived scalars, the number of unusual voxels in each subregion, normalized by the total number of voxels in the CC mask, was compared across groups using Kruskal–Wallis tests followed by post hoc pairwise comparisons. Statistical significance threshold was set at 0.05 after Bonferroni correction for multiple comparison.

Finally, we evaluated the diagnostic potential of V1 alterations in detecting iNPH compared to AD and PSP, and compared it with CC volume from the same regions. Using the 'caret' package available in R (version 4.0.2 for Mac), we trained different random forest classifiers to distinguish between iNPH and AD, between iNPH and PSP and between AD and PSP, and compared their performances using ROC analysis. Models were constructed based on: (i) the number of unusual V1 voxels in CC subregions where a significant difference between iNPH and other groups was found (independent variables); (ii) volume drawn from the same regions. The different models were evaluated and compared using ROC curves and the area under the curve (AUC) with 95% confidence intervals.

Results

The demographic and clinical characteristics of the patients are shown in Table 1. There was no difference in the age and sex distribution across groups. Disease duration was significantly lower in AD compared to the other two disease groups. All disease groups showed significantly lower MMSE scores compared to pooled healthy controls.

Patients with definite iNPH ($N = 13$) had significantly lower age at examination compared to those with MR-support diagnosis (definite iNPH = 13, mean age ± sd = 73.2 ± 6.0; MRsupport iNPH = 10, mean age ± sd = 80.2 ± 4.1; p value = 0.005). Unsurprisingly, age at onset also followed a similar trend, although not reaching significance (definite iNPH = 13, mean age at onset ± sd = 69.6 ± 7.8; MRsupport iNPH = 10, mean age at onset ± sd = 75.3 ± 4.0; p value = 0.06).

We observed different topographical distributions of changes in the CC: Fig. 2 shows that patients with iNPH presented V1 alterations in the midsagittal portion of the splenium, which differed significantly from patients with AD and PSP (in both post hoc comparisons, Bonferroni-corrected p value < 0.01). On the other hand, Fig. 3 shows that the number of voxels with significantly increased MD values compared to the control distributions was steady across the midsagittal profile, with iNPH and PSP significantly more affected than AD in the CC body (in both post hoc comparisons, Bonferroni-corrected p value < 0.01). Finally, Fig. 4 shows that the FA profile was similarly altered across all three patients' groups compared to the control distribution of FA values. Supplementary material includes the results of the analysis for AxD, rD and V2. As expected, rD and AxD showed alterations very similar to those detected with MD. The pattern of changes in V2, instead, resembled that found using FA, with peaks of alterations in the splenium and genu. However, no significant difference in the number of altered voxels was found between groups across the CC profile.

Figure 5 shows the main results of ROC analysis. The alterations of V1 in the splenium represented the best predictor of iNPH [$AUC_{iNPH\ vs\ PSP} = 0.88$ (0.77–1); $AUC_{iNPH\ vs\ AD} = 0.88$ (0.76–1)], even compared to more common and established measurements such as the callosal volume from the same region [$AUC_{iNPH\ vs\ PSP} = 0.74$ (0.58–0.90); $AUC_{iNPH\ vs\ AD} = 0.79$ (0.67–0.93)]. As expected, altered V1 voxels did not contribute to the differentiation of AD versus PSP [AUC = 0.54 (0.38–0.70)], where instead volume performed better [AUC = 0.72 (0.57–0.87)].

Discussion

Our study provides evidence that principal diffusion direction (V1) analysis can be successfully applied to a diagnostic challenge comparing three disorders (iNPH, AD, PSP) that share several clinical and radiological symptoms. The proposed method for semi-automated analysis of callosal integrity using V1 was able to identify microstructural alterations across these different neurological disorders that were not detectable using only volume measurements or common DTI metrics. In particular, alterations of V1 orientation in the CC splenium were specific to patients with iNPH, and the number of voxels characterized by altered V1 provided the highest AUC when differentiating iNPH from the other diseases (but not when comparing AD and PSP, as expected), thus also outperforming volumetric measurements drawn from the same region.

While FA and MD were altered in AD compared to healthy controls, we observed that (i) the orientation of V1 was not altered in these patients and (ii) the extent of the

Table 1 Demographic and clinical characteristics of the cohort

	HC ($N = 37$)	iNPH ($N = 23$)	PSP ($N = 27$)	AD ($N = 35$)	p value
Age (years)	75.8 ± 4.5	76.2 ± 6.2	72.7 ± 6.5	74.4 ± 9.2	0.21
Sex (M/F)	23/14	21/2	19/8	22/13	0.08
Age at onset (years)	–	72.0 ± 7.0	69.2 ± 6.6	72.5 ± 9.5	0.11
MMSE, median (range)	28 (25–30)	22 (12–29)	23 (6–29)	24 (20–26)	< 0.001
Evans index, median (range)	0.28 (0.21–0.33)	0.37 (0.33–0.57)	0.31 (0.22–0.36)	0.34 (0.23–0.47)	0.04

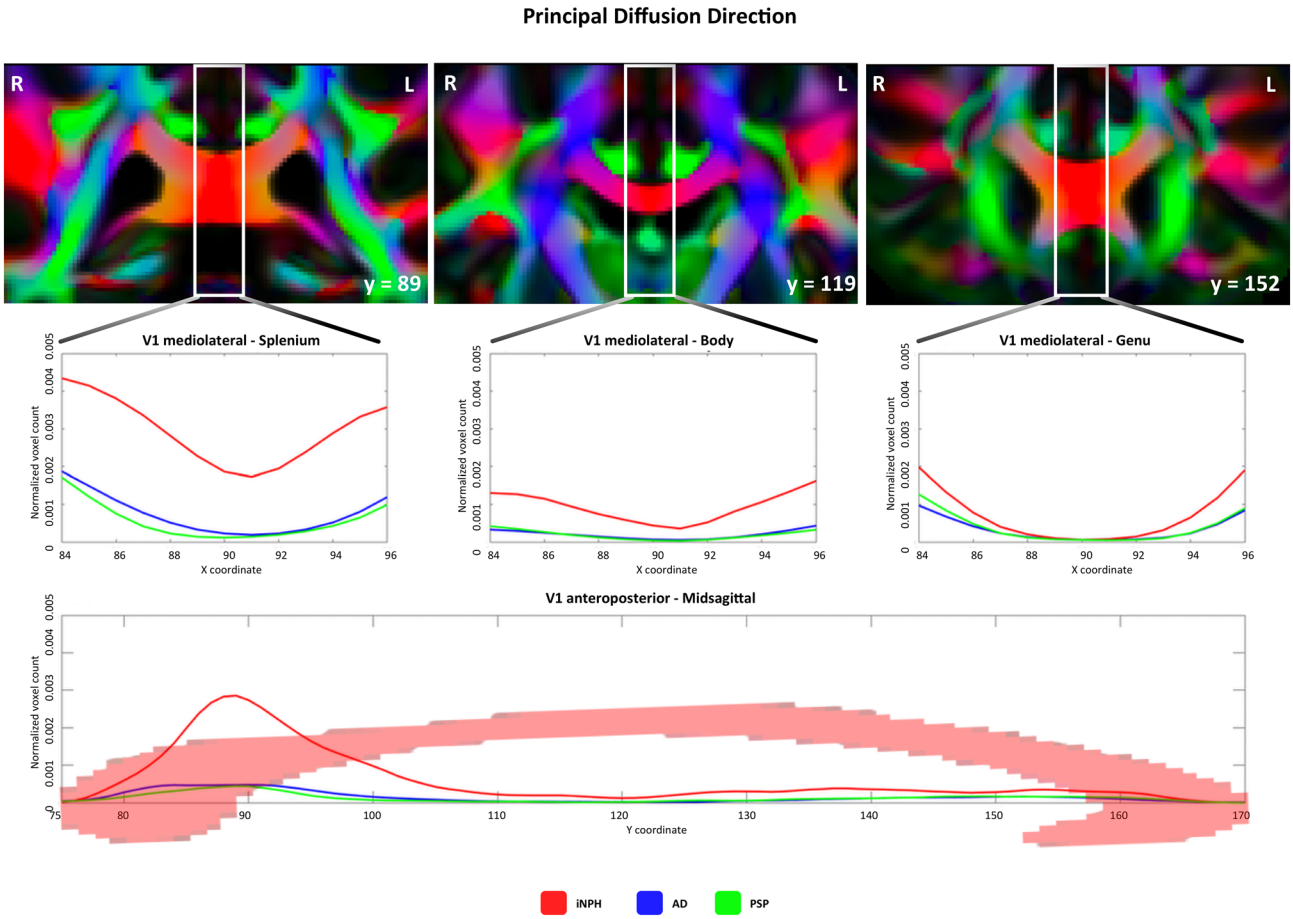

Fig. 2 Top row: CC splenium, body and genu in the coronal plane of V1-color-coded FA template. Middle row: altered V1 voxel count compared to control distribution along the anteroposterior axis (z-scores for both theta and phi values > 2.5 or < − 2.5). Bottom row: altered V1 voxel count along the mediolateral axis in CC subregions. *V1* principal diffusion direction; *FA* fractional anisotropy; *iNPH* idiopathic normal pressure hydrocephalus; *AD* Alzheimer's disease; *PSP* progressive supranuclear palsy

region in which MD was altered was significantly smaller compared to patients with iNPH and PSP. In the light of this, analysis of the differential involvement of V1 distribution across neurodegenerative (AD, PSP) and non-degenerative diseases (such as iNPH) could shed light on the different mechanisms that underlie tissue damage. Our hypothesis is that, while CC fibers are damaged in PSP and AD due to Wallerian degeneration, the frequently observed CC damage in iNPH could be due to the pressure that the ventricle exerts on the bundle.

It was recently demonstrated that iNPH patients can be accurately distinguished from PSP patients using a simple linear measurement of ventricle dilation, the magnetic resonance hydrocephalic index [3]. Compared to our proposed method, linear measurements are surely easier and leaner to apply in clinical practice, and also require minimum technical assets. In turn, our method is more sophisticated and computationally demanding, since it needs an off-line workstation to process MRI scans after the acquisition session, as well as an expert researcher to run the code and interpret results. On the other hand, our method was able to identify diffusion imaging characteristics specific to iNPH compared to both PSP and AD patients, which also outperformed more conventional metrics in the task of distinguishing these disorders. It is also worth noting that, since their research hypothesis was more focused on parkinsonian syndromes, linear measurements proposed in the aforementioned study were tested in patients with AD, which could have negatively influenced the results due to the severe ventricular dilation frequently observed as a feature of the disease.

The choice of CC as a region of interest lays in its key role in health and pathology, as well as in its microstructural characteristics. Traditional DTI metrics have been found affected in several neurological disorders, such as AD, Parkinson's disease and atypical parkinsonian syndromes, epilepsy, and multiple sclerosis [6, 22–26]. All these disorders have different, sometimes unknown, etiologies; however, existing studies reported similar patterns of FA and MD

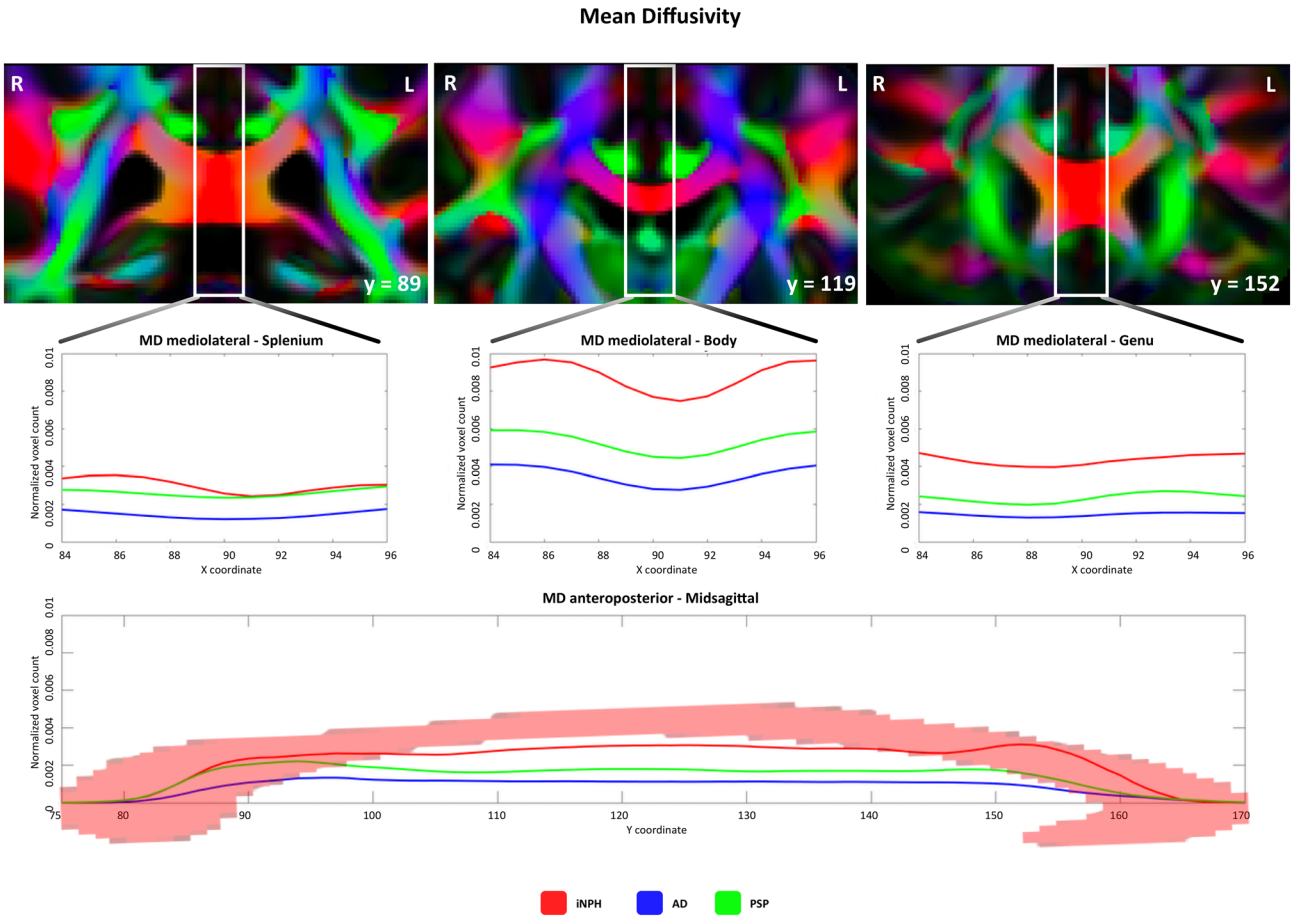

Fig. 3 Top row: CC splenium, body and genu in the coronal plane of V1-color-coded FA template. Middle row: altered MD voxel count compared to control distribution along the anteroposterior axis (mean and SD for controls = 0.0014 ± 0.0004 mm^2/s; for each voxel, *z*-score of the corresponding MD value was > 2.5 or < 2.5). Bottom row: altered MD voxel count along the mediolateral axis in CC subregions. *MD* mean diffusivity; *V1* principal diffusion direction; *FA* fractional anisotropy; *iNPH* idiopathic normal pressure hydrocephalus; *AD* Alzheimer's disease; *PSP* progressive supranuclear palsy

alterations across the CC region, which are likely driven by different pathological mechanisms (e.g., neurodegeneration, demyelination, abnormal electrophysiological activity). In the majority of these studies, either atrophy or microstructural alterations of the bundle or its subregions have been reported. In AD, diffusivity and FA changes in the genu and splenium have been described and associated with cognitive performance [6, 27, 28]. In PSP and its subtypes, widespread white matter damage, also involving the callosal bundle, has been measured using tract-based spatial statistics [7, 29]. In iNPH, diffusion metrics of CC and corticospinal tract have been frequently found altered compared to healthy controls and other neurodegenerative diseases such as AD [4].

Overall, while these three disorders all have different etiology and histopathological outcomes, existing DTI studies presented very similar patterns of callosal alterations, due to the well-known limitation of tensor-derived scalars, which lack specificity to the underlying pathological processes. Interestingly, our study demonstrated that a thorough analysis of both scalar and vector characteristics of the diffusion tensor is able to uncover disease-related differences that may otherwise go undetected.

The proposed pipeline is semi-automated, since it requires user intervention only for the quality check of image registration and CC segmentation. It was successfully applied to both multi-site data from the ADNI database and across different acquisition protocols. Image pre-processing only involved rigid-body alignment to standard space, to avoid using nonlinear deformations on brain structures severely affected by disease-related morphological changes. In these cases, in fact, nonlinear registration might fail and result in misalignment and excessive distortion, consequently invalidating the validity and robustness of any further processing of data. Another strength of our proposed method is that it was designed for single-shell data with a relatively

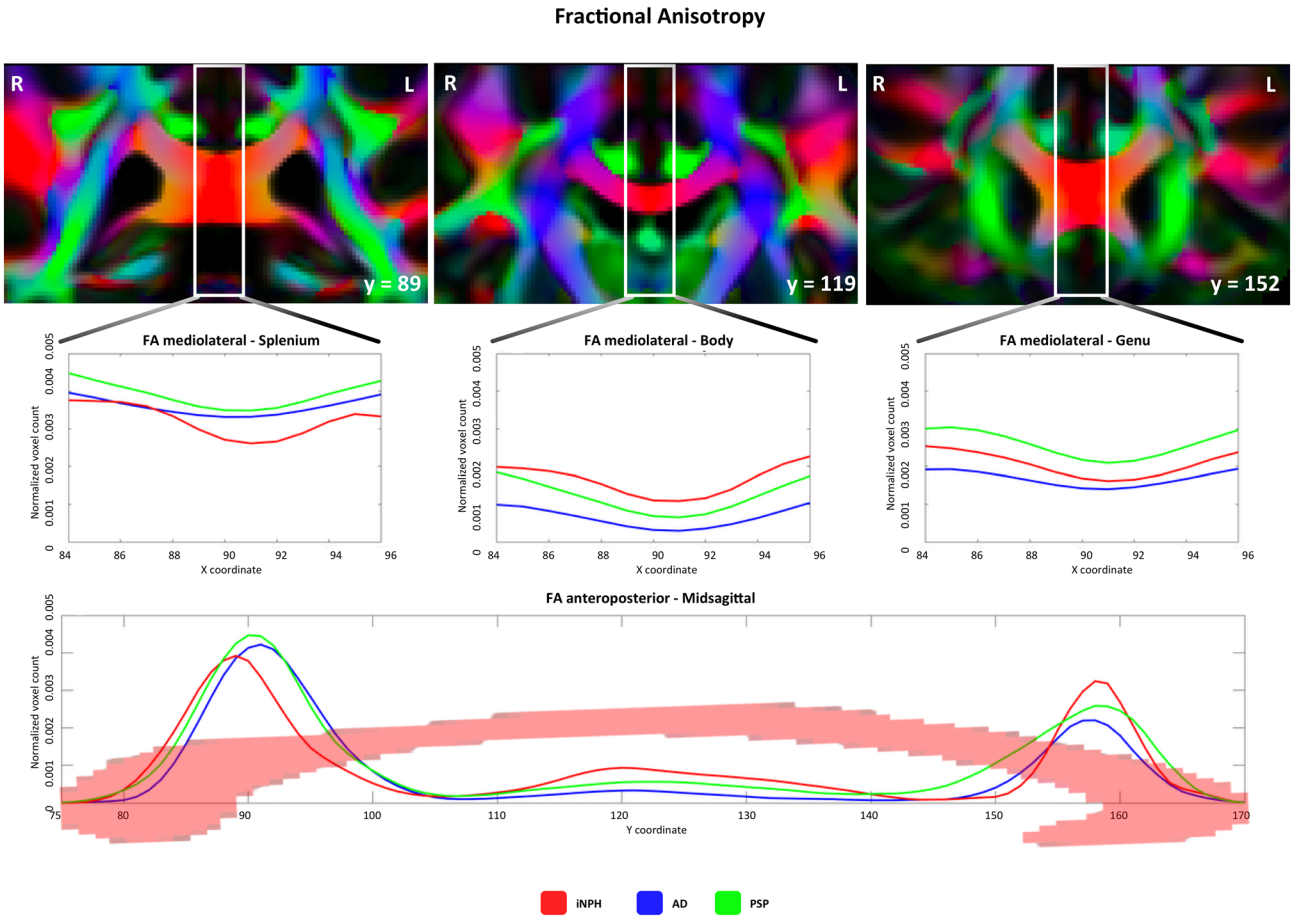

Fig. 4 Top row: CC splenium, body and genu in the coronal plane of V1-color-coded FA template. Middle row: altered FA voxel count compared to control distribution along the anteroposterior axis (mean and SD for controls = 0.54 ± 0.06; for each voxel, z-score of the corresponding FA value was > 2.5 or < 2.5). Bottom row: altered FA voxel count along the mediolateral axis in CC subregions. *V1* principal diffusion direction; *FA* fractional anisotropy; *iNPH* idiopathic normal pressure hydrocephalus; *AD* Alzheimer's disease; *PSP* progressive supranuclear palsy

low number of directions, to take into account its possible future application in routine clinical practice. On the other hand, it can also be easily applied to more sophisticated diffusion models that estimate the principal diffusion direction based on more complex acquisition schemes.

Obviously, this study has limitations. First, the sample sizes of the different groups are relatively small. However, all patients and healthy controls were carefully examined to exclude potential confounding factors. Second, the processing pipeline is quite complex, compared to other manual linear measurements more suitable for clinical practice. Third, despite our encouraging results, it is still extremely difficult to univocally associate DTI-derived changes with specific biological changes, without a spatially matching postmortem examination of cases.

Conclusions

In conclusion, this study highlights that investigating the principal diffusion direction in the brain is a promising and feasible approach to better describe changes in the brain caused by non-degenerative disorders such as iNPH, which is a very controversial clinical entity that might be easily misdiagnosed. Future studies will focus on (a) V1 distribution before and after shunting procedures, used to reduce cerebrospinal fluid pressure in iNPH, to test whether

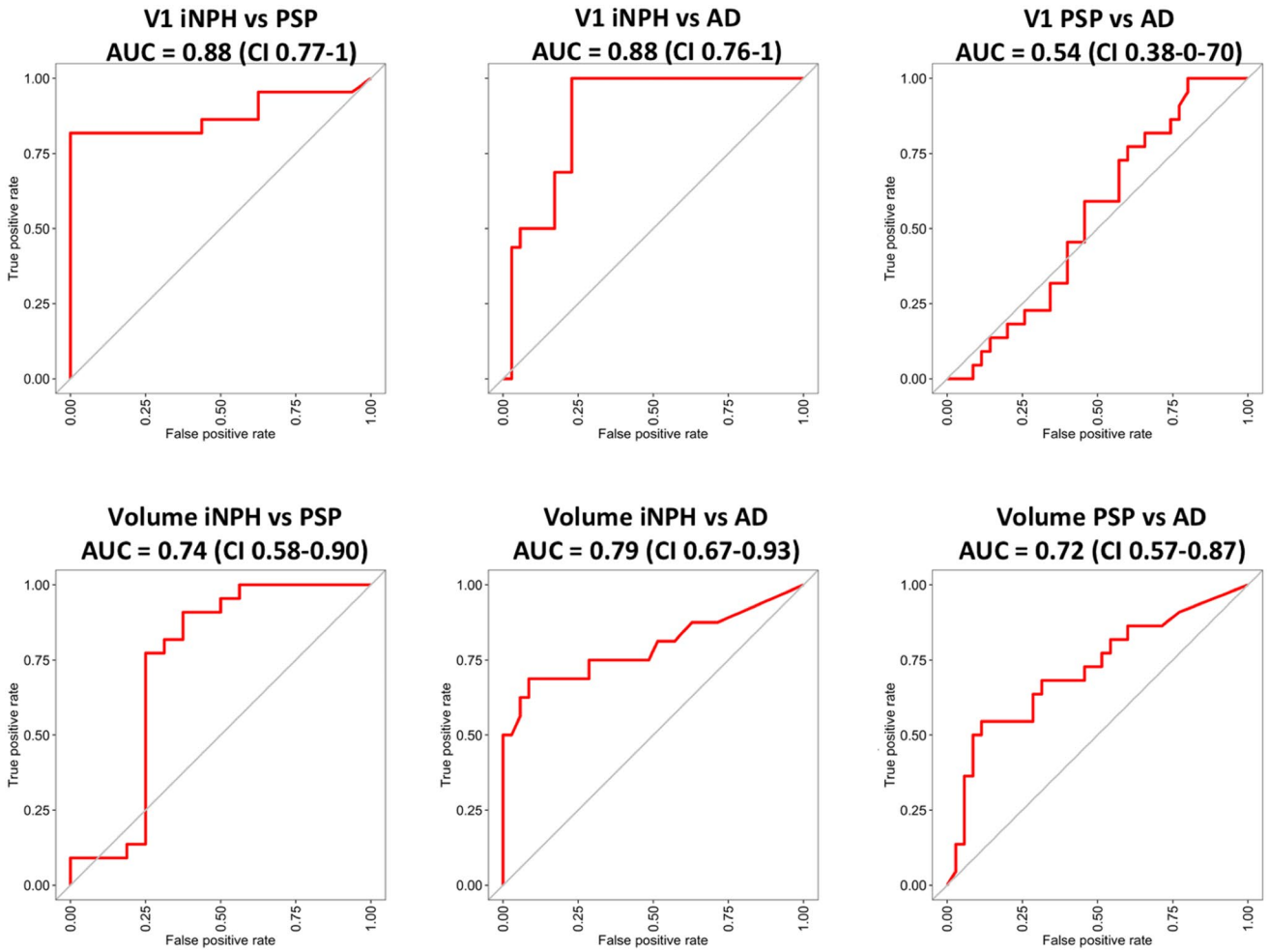

Fig. 5 ROC curves with 95% confidence intervals relative to the use of altered V1 in the splenium (top row) or splenial volume (bottom row) for iNPH versus PSP (first column), iNPH versus AD (second column) and AD versus PSP (third column). Number of patients: iNPH patients were 23, PSP patients were 27, and AD patients were 35. *V1* principal diffusion direction; *iNPH* idiopathic normal pressure hydrocephalus; *AD* Alzheimer's disease; *PSP* progressive supranuclear palsy

alterations are reversible and associated with surgical outcome; (b) generalizability of the method over independent cohorts.

Supplementary Information The online version contains supplementary material available at https://doi.org/10.1007/s00415-021-10762-9.

Author contributions MEC: conceptualization, methodology, software, validation, formal analysis, visualization, writing—original draft. AQ: conceptualization, data curation, investigation, writing—original draft. AM: resources, investigation. DLT: resources, investigation. AQ: conceptualization, writing—review & editing, supervision, project administration.

Funding No funding was received for conducting this study.

Availability of data and material The data that support the findings of this study are available on reasonable request from the corresponding author. The data are not publicly available due to privacy or ethical restrictions.

Code availability The code developed for this study is available on reasonable request from the corresponding author.

Declarations

Conflicts of interest The authors have no relevant financial or non-financial interests to disclose.

Ethics approval All local study procedures were carried out in accordance with the Declaration of Helsinki and ethical aspects were

approved by the institutional review board (Magna Graecia University review board, Catanzaro, Italy). Each ADNI recruitment site received approval from an institutional review board or ethics committee on human experimentation before ADNI study initiation.

Consent to participate Written informed consent for research was obtained from all individuals participating in the study.

Consent to publish Not applicable.

References

1. Quattrone A, Nicoletti G, Messina D, Fera F, Condino F, Pugliese P, Lanza P, Barone P, Morgante L, Zappia M, Aguglia U, Gallo O (2008) MR imaging index for differentiation of progressive supranuclear palsy from Parkinson disease and the Parkinson variant of multiple system atrophy. Radiology 246(1):214–221. https://doi.org/10.1148/radiol.2453061703
2. Nigro S, Antonini A, Vaillancourt DE, Seppi K, Ceravolo R, Strafella AP, Augimeri A, Quattrone A, Morelli M, Weis L, Fiorenzato E, Biundo R, Burciu RG, Krismer F, McFarland NR, Mueller C, Gizewski ER, Cosottini M, Del Prete E, Mazzucchi S, Quattrone A (2020) Automated MRI classification in progressive supranuclear palsy: a large international cohort study. Mov Disord 35(6):976–983. https://doi.org/10.1002/mds.28007
3. Quattrone A, Sarica A, La Torre D, Morelli M, Vescio B, Nigro S, Barbagallo G, Nisticò R, Salsone M, Arcuri PP, Novellino F, Bianco MG, Arabia G, Cascini G, Quattrone A (2020) Magnetic resonance imaging biomarkers distinguish normal pressure hydrocephalus from progressive supranuclear palsy. Mov Disord 35(8):1406–1415. https://doi.org/10.1002/mds.28087
4. Siasios I, Kapsalaki EZ, Fountas KN, Fotiadou A, Dorsch A, Vakharia K, Pollina J, Dimopoulos V (2016) The role of diffusion tensor imaging and fractional anisotropy in the evaluation of patients with idiopathic normal pressure hydrocephalus: a literature review. Neurosurg Focus 41(3):E12. https://doi.org/10.3171/2016.6.FOCUS16192
5. Tan K, Meiri A, Mowrey WB, Abbott R, Goodrich JT, Sandler AL, Suri AK, Lipton ML, Wagshul ME (2018) Diffusion tensor imaging and ventricle volume quantification in patients with chronic shunt-treated hydrocephalus: a matched case-control study. J Neurosurg 129(6):1611–1622. https://doi.org/10.3171/2017.6.JNS162784
6. Di Paola M, Di Iulio F, Cherubini A, Blundo C, Casini AR, Sancesario G, Passafiume D, Caltagirone C, Spalletta G (2010) When, where, and how the corpus callosum changes in MCI and AD: a multimodal MRI study. Neurology 74(14):1136–1142. https://doi.org/10.1212/WNL.0b013e3181d7d8cb
7. Quattrone A, Caligiuri ME, Morelli M, Nigro S, Vescio B, Arabia G, Nicoletti G, Nisticò R, Salsone M, Novellino F, Barbagallo G, Vaccaro MG, Sabatini U, Vescio V, Stanà C, Rocca F, Caracciolo M, Quattrone A (2019) Imaging counterpart of postural instability and vertical ocular dysfunction in patients with PSP: a multimodal MRI study. Parkinsonism Relat Disord 63:124–130. https://doi.org/10.1016/j.parkreldis.2019.02.022
8. Wheeler-Kingshott CA, Cercignani M (2009) About "axial" and "radial" diffusivities. Magn Reson Med 61(5):1255–1260. https://doi.org/10.1002/mrm.21965
9. Wu YC, Field AS, Chung MK, Badie B, Alexander AL (2004) Quantitative analysis of diffusion tensor orientation: theoretical framework. Magn Reson Med 52(5):1146–1155. https://doi.org/10.1002/mrm.20254
10. Schwartzman A, Dougherty RF, Taylor JE (2005) Cross-subject comparison of principal diffusion direction maps. Magn Reson Med 53(6):1423–1431. https://doi.org/10.1002/mrm.20503
11. Aboitiz F, Scheibel AB, Fisher RS, Zaidel E (1992) Fiber composition of the human corpus callosum. Brain Res 598(1–2):143–153. https://doi.org/10.1016/0006-8993(92)90178-c
12. Mori E, Ishikawa M, Kato T, Kazui H, Miyake H, Miyajima M, Nakajima M, Hashimoto M, Kuriyama N, Tokuda T, Ishii K, Kaijima M, Hirata Y, Saito M, Arai H, Japanese Society of Normal Pressure Hydrocephalus (2012) Guidelines for management of idiopathic normal pressure hydrocephalus: second edition. Neurol Med Chir (Tokyo) 52(11):775–809. https://doi.org/10.2176/nmc.52.775
13. Höglinger GU, Respondek G, Stamelou M, Kurz C, Josephs KA, Lang AE, Mollenhauer B, Müller U, Nilsson C, Whitwell JL, Arzberger T, Englund E, Gelpi E, Giese A, Irwin DJ, Meissner WG, Pantelyat A, Rajput A, van Swieten JC, Troakes C, Antonini A, Bhatia KP, Bordelon Y, Compta Y, Corvol JC, Colosimo C, Dickson DW, Dodel R, Ferguson L, Grossman M, Kassubek J, Krismer F, Levin J, Lorenzl S, Morris HR, Nestor P, Oertel WH, Poewe W, Rabinovici G, Rowe JB, Schellenberg GD, Seppi K, van Eimeren T, Wenning GK, Boxer AL, Golbe LI, Litvan I, Movement Disorder Society-endorsed PSP Study Group (2017) Clinical diagnosis of progressive supranuclear palsy: the movement disorder society criteria. Mov Disord 32(6):853–864. https://doi.org/10.1002/mds.26987
14. http://adni.loni.usc.edu/wp-content/uploads/2008/07/adni2-procedures-manual.pdf. Accessed 17 May 2021
15. http://adni.loni.usc.edu/methods/mri-tool/mri-acquisition/. Accessed 17 May 2021
16. Shaw LM, Figurski M, Waligorska T and Trojanowski JQ (2016) An overview of the first 8 ADNI CSF batch analyses. https://adni.bitbucket.io/reference/docs/UPENNBIOMK_MASTER/ADNI_Methods_Template_Shaw%20Figurski%20Waligorska%20Trojanowski%20overview%20for%20CSF%20Ab1-42%20tau%20and%20ptau181%20AlzBio3%20immunoassay%20datav3%20(5).pdf. Accessed 17 May 2021
17. https://ida.loni.usc.edu/pages/access/studyData.jsp?categoryId=14&subCategoryId=47. Accessed 17 May 2021
18. Jenkinson M, Beckmann CF, Behrens TE, Woolrich MW, Smith SM (2012) FSL Neuroimage 62(2):782–790. https://doi.org/10.1016/j.neuroimage.2011.09.015
19. Rockel C, Noseworthy MD (2016) An exploration of diffusion tensor eigenvector variability within human calf muscles. J Magn Reson Imaging 43:190–202. https://doi.org/10.1002/jmri.24957
20. Catani M, Howard RJ, Pajevic S, Jones DK (2002) Virtual in vivo interactive dissection of white matter fasciculi in the human brain. Neuroimage 17(1):77–94. https://doi.org/10.1006/nimg.2002.1136
21. Nicoletti G, Caligiuri ME, Cherubini A, Morelli M, Novellino F, Arabia G, Salsone M, Quattrone A (2017) A fully automated, atlas-based approach for superior cerebellar peduncle evaluation in progressive supranuclear palsy phenotypes. Am J Neuroradiol 38(3):523–530. https://doi.org/10.3174/ajnr.A5048
22. Bohnen NI, Albin RL (2011) White matter lesions in Parkinson disease. Nat Rev Neurol 7(4):229–236. https://doi.org/10.1038/nrneurol.2011.21
23. Salsone M, Caligiuri ME, Vescio V, Arabia G, Cherubini A, Nicoletti G, Morelli M, Quattrone A, Vescio B, Nisticò R, Novellino F, Cascini GL, Sabatini U, Montilla M, Rektor I, Quattrone A (2019) Microstructural changes of normal-appearing white matter in vascular Parkinsonism. Parkinsonism Relat Disord 63:60–65. https://doi.org/10.1016/j.parkreldis.2019.02.046
24. Caligiuri ME, Labate A, Cherubini A, Mumoli L, Ferlazzo E, Aguglia U, Quattrone A, Gambardella A (2016) Integrity of the

corpus callosum in patients with benign temporal lobe epilepsy. Epilepsia 57(4):590–596. https://doi.org/10.1111/epi.13339
25. Barone S, Caligiuri ME, Valentino P, Cherubini A, Chiriaco C, Granata A, Filippelli E, Tallarico T, Nisticò R, Quattrone A (2018) Multimodal assessment of normal-appearing corpus callosum is a useful marker of disability in relapsing-remitting multiple sclerosis: an MRI cluster analysis study. J Neurol 265(10):2243–2250. https://doi.org/10.1007/s00415-018-8980-y
26. Caligiuri ME, Barone S, Cherubini A, Augimeri A, Chiriaco C, Trotta M, Granata A, Filippelli E, Perrotta P, Valentino P, Quattrone A (2014) The relationship between regional microstructural abnormalities of the corpus callosum and physical and cognitive disability in relapsing-remitting multiple sclerosis. Neuroimage Clin 7:28–33. https://doi.org/10.1016/j.nicl.2014.11.008
27. Wang PN, Chou KH, Chang NJ, Lin KN, Chen WT, Lan GY, Lin CP, Lirng JF (2014) Callosal degeneration topographically correlated with cognitive function in amnestic mild cognitive impairment and Alzheimer's disease dementia. Hum Brain Mapp 35(4):1529–1543. https://doi.org/10.1002/hbm.22271
28. Teipel S, Grothe MJ, Zhou J, Sepulcre J, Dyrba M, Sorg C, Babiloni C (2016) Measuring cortical connectivity in Alzheimer's disease as a brain neural network pathology: toward clinical applications. J Int Neuropsychol Soc 22(2):138–163. https://doi.org/10.1017/S1355617715000995
29. Caso F, Agosta F, Ječmenica-Lukić M, Petrović I, Meani A, Kostic VS, Filippi M (2018) Progression of white matter damage in progressive supranuclear palsy with predominant parkinsonism. Parkinsonism Relat Disord 49:95–99. https://doi.org/10.1016/j.parkreldis.2018.01.001